

Normalized Conditional Mutual Information Surrogate Loss for Deep Neural Classifiers

Linfeng Ye^{§‡*}, Zhixiang Chi^{‡*}, Konstantinos N. Plataniotis[‡], En-hui Yang^{§†}

[§]Department of Electrical and Computer Engineering, University of Waterloo, Waterloo, Canada

[‡]The Edward S. Rogers Sr. Department of Electrical and Computer Engineering, University of Toronto, Toronto, Canada

Email: {l44ye, ehyang}@uwaterloo.ca[§], {chizhixi, kostas}@ece.utoronto.ca[‡]

Abstract—In this paper, we propose a novel information-theoretic surrogate loss—normalized conditional mutual information (NCMI)—as a drop-in alternative to the de facto cross-entropy (CE) for training deep neural network (DNN)-based classifiers. We first observe that the model’s NCMI is inversely proportional to its accuracy. Building on this insight, we introduce an alternating algorithm to efficiently minimize the NCMI. Across image recognition and whole-slide imaging (WSI) subtyping benchmarks, NCMI-trained models surpass state-of-the-art losses by substantial margins at a computational cost comparable to that of CE. Notably, on ImageNet, NCMI yields a 2.77% top-1 accuracy improvement with ResNet-50 comparing to the CE; on CAMELYON-17, replacing CE with NCMI improves the macro-F1 by 8.6% over the strongest baseline. Gains are consistent across various architectures and batch sizes, suggesting that NCMI is a practical and competitive alternative to CE. All code and data are publicly available at <https://github.com/Linfeng-Ye/NCMI>.

Index Terms—Alternating minimization, surrogate loss, deep learning, conditional mutual information

I. INTRODUCTION

Cross entropy (CE), first introduced by Cox [1] for binary classification in the 1950s as the objective function for analyzing binary sequences, has become the de facto objective function for the most modern supervised learning algorithm for classification, while its capability for multi-class classification has not been justified until very recently [2]. In practice, CE minimizes the negative log-likelihood with one-hot targets, which geometrically pulls predictions toward the corners of the simplex.

A large body of work augments CE with additional regularizers or proposes ad-hoc alternatives that empirically compete with CE. Specifically, orthogonal projection loss (OPL) [3] augments CE by maximizing cosine similarity among intra-class features while driving inter-class similarities toward zero; Squentropy [4] applies an ℓ_2 penalty to non-ground-truth entries of the output probability distribution, supervised contrastive learning (SupCon) [5] extends the infoNCE [6] loss to the supervised setting by treating all samples in the batch samples sharing the anchor’s label as positives, and SquareLoss [7] argues that mean-squared-error (MSE) loss, with careful hyperparameter tuning, can match or even outperform CE. However, these approaches typically remain CE-centric; their

performance depends on CE, while the auxiliary terms are ineffective on their own, require extensive hyperparameter tuning, or rely on very large batch sizes to realize their gains.

We note that in previous approaches, the learning process can be regarded as optimizing the model so that the output clusters are pulled toward predefined, corresponding distributions on the probability simplex. In this paper, we aim to answer the following question:

Instead of pulling output toward pre-defined target distributions, can we facilitate the learning by shaping the output distribution to be concentrated within classes and well-separated across classes using an information-theoretic principle?

To this end, following [2], we model the DNN-based classification task as a three-state Markov chain, as illustrated in Figure 1. We quantify the concentration of the output distribution using the conditional mutual information (CMI) between the input and output, conditioned on the ground-truth label, and we quantify separation with Γ . We then define the normalized conditional mutual information (NCMI) as the ratio between the CMI and Γ . During training, instead of maximizing the log-likelihood (i.e., minimizing CE), we train the model to minimize its NCMI. After training, we evaluate the model using centroid-based decisions, comparing its outputs to class centroids and via linear probing. Empirically, NCMI outperforms prior state-of-the-art losses and serves as an efficient surrogate for classification. The key contributions are as follows:

- We propose a new CE alternative named NCMI, for training DNN-based classifiers.
- To minimize the NCMI, we introduce a novel alternating optimization algorithm that minimizes the NCMI loss.
- To evaluate the NCMI’s effectiveness, we conduct comprehensive experiments on two natural-image datasets, namely, CIFAR-100 [8] ImageNet [9] and two whole-slide image (WSI) datasets, CAMELYON-17 [10] and BRACS [11]. Although modern DNNs and optimization tricks are tailored to CE-based surrogates, NCMI achieves state-of-the-art classification performance across all benchmarks.

II. RELATED WORK

Within the existing literature, cross-entropy (CE) and its variants are the de facto objectives for classification. Several works have attempted to improve CE. Empirical studies report that DNNs with compact feature clusters usually outperform

* Equal contribution.

† Corresponding author.

$$Y \xrightarrow{P_{X|Y}(\cdot|y)} X \xrightarrow{(\sigma \circ f)(\cdot)} \mathcal{P}$$

Fig. 1. Mappings from the label space Y to the input space X , and from the input space to a output space \hat{Y} . Input x are sampled from the class $Y = y$ according to the $P_{X|Y}(\cdot|y)$. This is further mapped by a DNN and a simplex-valued function to an output probability distribution $p \in \mathcal{P}$.

those with sparse clusters [12]–[14]. These insights have been further analyzed under the Gaussian-mixture assumption on the feature distribution [15]. Building on this line of work, subsequent works augment CE with regularizers to strengthen intra-class concentration and inter-class margins. Specifically, Hui et al. [4] add an ℓ_2 penalty to the non-ground-truth entries of the predicted probability distribution, and OPL [16] explicitly clusters same-class features while enforcing orthogonality between different classes in the penultimate layer.

Another line of work improves classification accuracy by modifying CE. Focal Loss [17] down-weights well-classified examples via a power transformation so training emphasizes hard instances. PolyLoss [18] reframes standard classification losses as polynomial expansions. Hui et al. propose SquareLoss [7], and empirically found that squared loss performs on par with or even outperforms CE on modern DNNs. Supervised contrastive learning (SuperCon) [5] pulls together same-class embeddings and pushes apart different-class embeddings, followed by a linear classifier trained on the frozen features. Further, to mitigate overconfident predictions, label smoothing (LS) [19] softens the one-hot targets, which can inadvertently produce compact class clusters [20]. AntiClass [21] replaces the one-hot target with a one-cold target to mitigate neural collapse.

In contrast, this paper studies the surrogate loss for classification through the lens of information theory. We view a DNN as a mapping from $x \in \mathbb{R}^d$ to $p \in \mathcal{P}^n$, and we train the model by directly minimizing its conditional mutual information.

III. NOTATION AND PRELIMINARIES

A. Notation

Scalars are denoted by non-bold letters (e.g. β), vectors by bold lowercase letter (e.g. a), the i -th entry of a vector a is written as a_i . We denote \mathcal{P}^n as the set of all n -dimensional probability distributions. For any two probability distributions $p, q \in \mathcal{P}^n$, the Kullback–Leibler (KL) divergence is defined as

$$D(p\|q) = \sum_{i=1}^n p_i \ln \frac{p_i}{q_i}, \quad (1)$$

where \ln denotes the logarithm with base e , write the CE of the one-hot probability distribution corresponding to y and q as $H(y, q) = -\ln q_y$. Let \mathcal{S} be a collection of simplex-valued functions on \mathbb{R}^n , i.e.

$$\mathcal{S} \subseteq \{ \sigma : \mathbb{R}^n \rightarrow \mathcal{P}^n \}, \quad (2)$$

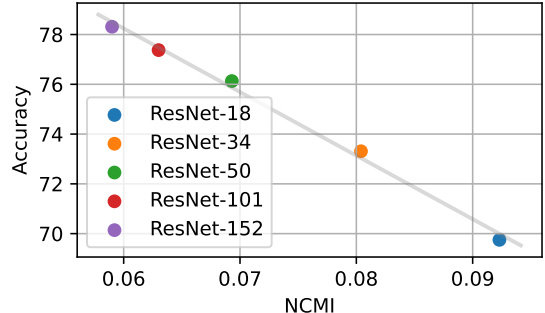


Fig. 2. The accuracy vs NCMI value over the validation set of pre-trained ResNet models on the ImageNet dataset.

specifically, we define normalized sigmoid function (NSF) σ^{NSF} and softmax function σ^{SM} as

$$\sigma^{NSF}(z)_j = \frac{\phi(z_j)}{\sum_{i=1}^n \phi(z_i)}, \quad \phi(z_i) = \frac{1}{1 + e^{z_i}}; \quad (3)$$

$$\sigma^{SM}(z)_i = \frac{e^{z_i}}{\sum_{i=1}^n e^{z_i}}, \quad \text{where } z \in \mathbb{R}^n. \quad (4)$$

Given a multi-class classification dataset \mathcal{D} , let $\mathcal{D}^y \subseteq \mathcal{D}$ denote the subset of samples labeled y .

B. Modeling Classification as a Markov Chain

In a classification task with c classes, a DNN f and a σ could be regarded as a mapping $(\sigma \circ f) : x \rightarrow p$, where $x \in \mathbb{R}^d$ is an input, and $p \in \mathcal{P}^n$ is the output probability distribution. Usually, $n = c$ when we use CE as the surrogate loss. Following [22], we can model the classification task as a three-state Markov chain, as depicted in Figure 1. As shown in [2], we empirically quantify the concentration of DNN’s output by

$$I(X; \mathcal{P}|Y) = \sum_y P_Y(y) \sum_x P_{X|Y}(x|y) \left[\sum_{i=1}^n p_i \ln \frac{p_i}{s_i^y} \right], \quad (5)$$

$$\text{where } s_i^y \triangleq \frac{1}{|\mathcal{D}^y|} \sum_{x \in \mathcal{D}^y} p_i, \quad \text{for } y \in Y. \quad (6)$$

Further, the separation of DNN’s output can be quantified as

$$\Gamma = \sum_{v \in Y} \sum_{x \in \mathcal{D}^v} I_{\{v \neq y\}} P_{X|Y}(x|v) \sum_{i=1}^n p_i \ln \frac{s_i^v}{p_i} \quad (7)$$

Ideally, we want $I(X; \mathcal{P}|Y = y)$ to be small while keeping Γ large. This leads us to consider the ratio between $I(X; \mathcal{P}|Y = y)$ and Γ .

$$\hat{I}(X; \mathcal{P}|Y) \triangleq \frac{I(X; \mathcal{P}|Y)}{\Gamma}. \quad (8)$$

We refer to $\hat{I}(X; \mathcal{P}|Y)$ as the normalized conditional mutual information (NCMI). To examine how NCMI relates to classification performance, we compute NCMI and top-1 accuracy for pretrained ResNet variants on the ImageNet validation set, as seen in the Figure 2. We observe a clear inverse linear relationship: models with lower NCMI achieve higher accuracy, with a Pearson correlation coefficient exceeding -0.997 . This suggests that, for a fixed DNN family, improving

performance is associated with simultaneously reducing both the error rate and the model’s NCMI during training.

Motivated by this observation, in the next section, we demonstrate that NCMI per se suffices for training DNN classifiers.

IV. METHODOLOGY

Previous discussions suggest a new surrogate loss for training DNN-based classifiers. Specifically, in the learning process, instead of minimizing the CE surrogate loss, which pulls the output toward predefined distributions, we aim to minimize $\hat{I}(X; \mathcal{P}|Y = y)$. The algorithm for minimizing the novel surrogate loss is outlined below.

A. Training DNN by minimizing NCMI

The optimization problem can be written as

$$\begin{aligned} \min_{\theta} \hat{I}(X; \mathcal{P}|Y) = \\ \min_{\theta} \frac{\sum_y P_Y(y) \sum_{\mathbf{x}} P_{X|Y}(\mathbf{x}|y) \left[\sum_{i=1}^n \mathbf{p}_i \ln \frac{\mathbf{p}_i}{\mathbf{s}_i^y} \right]}{\sum_{v \in Y} \sum_{\mathbf{x} \in \mathcal{D}^v} I_{\{v \neq y\}} P_{X|Y}(\mathbf{x}|v) \sum_{j=1}^n \mathbf{p}_j \ln \frac{\mathbf{s}_j^v}{\mathbf{p}_j}} \quad (9) \end{aligned}$$

We notice that the objective in Equation (9) is not amenable to parallel computation via GPU due to the dependency of $\hat{I}(X; \mathcal{P}|Y)$ on the centroid \mathbf{s}^y of each cluster corresponding to $Y = y$ (see Equation (6)). To overcome this, we introduce a dummy distribution $\mathbf{q}^y \in \mathcal{P}^n$ for each $y \in [C]$ and convert it into a double minimization problem.

$$\begin{aligned} \min_{\theta} \frac{\sum_y P_Y(y) \sum_{\mathbf{x}} P_{X|Y}(\mathbf{x}|y) \left[\sum_{i=1}^n \mathbf{p}_i \ln \frac{\mathbf{p}_i}{\mathbf{s}_i^y} \right]}{\sum_{v \in Y} \sum_{\mathbf{x} \in \mathcal{D}^v} I_{\{v \neq y\}} P_{X|Y}(\mathbf{x}|v) \sum_{i=1}^n \mathbf{p}_i \ln \frac{\mathbf{s}_i^v}{\mathbf{p}_i}} \equiv \\ \min_{\mathbf{q}^v, v \in [C]} \min_{\theta} \frac{\sum_y P_Y(y) \sum_{\mathbf{x}} P_{X|Y}(\mathbf{x}|y) \left[\sum_{i=1}^n \mathbf{p}_i \ln \frac{\mathbf{p}_i}{\mathbf{q}_i^y} \right]}{\sum_{v \in Y} \sum_{\mathbf{x} \in \mathcal{D}^v} I_{\{v \neq y\}} P_{X|Y}(\mathbf{x}|v) \sum_{j=1}^n \mathbf{p}_j \ln \frac{\mathbf{q}_j^v}{\mathbf{p}_j}} \quad (10) \end{aligned}$$

By reformulating the single minimization problem as a double minimization problem, Equation (10) suggests an alternating algorithm, in which we use gradient descent to minimize the objective function with respect to the model’s parameters θ and centroids $\mathbf{q}^v, v \in [C]$ iteratively.

In the next section, we present the details of the training recipe and the evaluation protocols used to assess the NCMI loss.

B. Implementation and evaluation protocols

In this section, we provide the implementation details for training using NCMI and present the evaluation protocols applied in our experiments.

a) *NCMI training*: A network f_{θ} ¹ maps input to a feature vector, followed by ℓ_2 normalization, which is further mapped to a probability distribution. To avoid the model’s output probability distribution collapsing to a single distribution, following

¹We use ResNet [23] for image recognition and multiple instance learning models [24] for whole slide image.

Algorithm 1 PyTorch-style pseudo-code of the proposed alternating algorithm for solving the optimization problem in Equation (10).

```

# model  $f_{\theta}$ ; centroid  $\xi$ ; momentum rate  $m$ ; temperature  $\tau$ ; centroid and model optimizer  $\text{optimizer}_{\xi}$ ,  $\text{optimizer}_{\theta}$ .
1: for  $\mathbf{x}, \mathbf{y}$  in loader do
2:    $\mathbf{z} \leftarrow f_{\theta}(\mathbf{x}) - \mathbf{c}$                                 #  $\mathbf{z}$ .shape:  $[B, D]$ 
3:    $\mathbf{z}' \leftarrow \text{L2NORMALIZE}(\mathbf{z})/\tau$  #  $\ell_2$  norm / temperature
4:    $\mathbf{c} \leftarrow m * \mathbf{c} + (1 - m) * \mathbf{z}.\text{mean(dim=0).detach()}$           #  $\mathbf{c}$ .shape:  $[1, D]$ 
5:    $\mathbf{p}, \mathbf{q} \leftarrow \sigma^{\text{NSF}}(\mathbf{z}'), \sigma^{\text{NSF}}(\xi)$           #  $\mathbf{p}$ .shape:  $[B, D]$ ;  $\mathbf{q}$ .shape:  $[C, D]$ 
6:   Calculate CMI according to Equation (5)                                # CMI.shape:  $[B, 1]$ 
7:   Calculate  $\Gamma$  according to Equation (7)                                #  $\Gamma$ .shape:  $[B, C]$ 
8:    $\text{optimizer}_{\xi}.\text{zero\_grad}()$ ,  $\text{optimizer}_{\theta}.\text{zero\_grad}()$ 
9:   loss  $\leftarrow (\mathbf{CMI}/\Gamma).\text{mean}()$ 
10:  loss.backward()
11:   $\text{optimizer}_{\xi}.\text{step}()$ ,  $\text{optimizer}_{\theta}.\text{step}()$ 
12: end for

```

the [25], [26], we center the feature, then scale it with a pre-defined temperature τ , then we use NSF to map the feature vectors to probability vectors. We present PyTorch-style [27] pseudo-code for NCMI implementation in Algorithm 1. Please refer to our code repository for full training details.

b) *Evaluation Protocols*: We evaluate the performance of the NCMI-trained model under two protocols: linear probing and decision-based on comparison with centroids.

Linear probing. We first evaluate the NCMI-trained model with the standard protocol by training a linear classifier on frozen features [5] using CE. We apply the same data augmentation as in the training process, freeze the model trained by NCMI, drop the σ^{NSF} , and train a linear classifier using stochastic gradient descent (SGD).

Decision based on comparison with centroids. We further evaluate the NCMI-trained model on unseen samples from the test set by comparing them with the centroid of each class. To this end, the NCMI trained model predicts output based on comparison with centroids, specifically, we calculate the KL divergence between its output distribution \mathbf{p} of the model and each centroid \mathbf{q}^v per class $D(\mathbf{p} \parallel \mathbf{q}^v)$, $v \in [C]$. Then the prediction is made based on the centroid with the smallest KL-divergence value.

V. EXPERIMENTS

To illustrate the effectiveness of NCMI and compare it with some state-of-the-art alternatives, a series of experiments was conducted. Specifically, we conduct experiments on two widely used natural image datasets, namely CIFAR-100 [8] and ImageNet [9], as well as two whole-slide image datasets, namely CAMELYON-17 [28] and BRACS [11]. In the tables, NCMI-LP and NCMI-CC denote NCMI evaluated with linear probing (LP) and with centroid comparison (CC), respectively.

TABLE I

TOP-1 VALIDATION ACCURACY ON CIFAR-100 FOR MODELS TRAINED WITH NCMI AND BASELINE METHODS, AVERAGED OVER THREE RANDOM SEEDS. CC DENOTES GREEDY PREDICTION VIA NEAREST-CENTROID COMPARISON; LP DENOTES LINEAR PROBING. THE BEST AND SECOND-BEST RESULTS ARE SHOWN IN **BOLD** AND UNDERLINED, RESPECTIVELY.

CIFAR-100				
Model	ResNet-18	ResNet-34	ResNet-50	ResNet-101
CE	75.44	76.42	76.96	77.39
LS	75.92	76.77	77.06	77.37
AntiClass	76.28	76.31	76.30	76.69
Squentropy	75.71	76.62	77.15	77.74
SquareLoss	75.10	76.62	77.15	77.74
PolyLoss	75.59	76.87	76.46	77.77
SupCon	73.00	74.53	74.88	75.77
SupCon (large BS)	-	-	77.04	-
Focal Loss	76.34	76.62	77.32	77.76
NCMI-CC (ours)	76.45	<u>76.97</u>	<u>77.50</u>	<u>77.81</u>
NCMI-LP (ours)	76.94	<u>77.34</u>	<u>77.76</u>	<u>78.23</u>

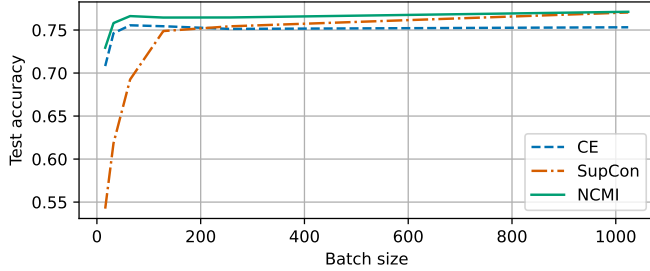


Fig. 3. ResNet-50 test accuracy on CIFAR-100 as a function of batch size. We evaluate batch sizes {16, 32, 64, 128, 256, 1024}; NCMI consistently outperforms CE and SupCon across all settings.

A. Experiments on CIFAR-100

The CIFAR-100 dataset contains 50-K training and 10-K test color images of resolution 32×32 , which are labeled for 100 classes.

To illustrate the effectiveness of NCMI, we have conducted experiments on models of varying sizes. Specifically, we have selected ResNet-18, ResNet-34, ResNet-50 and ResNet-101 for evaluation, and compare NCMI with respect to 8 benchmark methods namely, CE, LS [19], AntiClass [21], Squentropy [4], SquareLoss [7], PolyLoss [18], SupCon [5] and Focal Loss [17].

For all surrogate losses, we use an SGD optimizer with a momentum of 0.9, a learning rate of 0.1, and a weight decay of 0.0005, along with a batch size of 64. We train the model for 240 epochs, and at epochs 60, 120, and 160, we reduce the current learning rate by a factor of 10. Since SupCon relies on a large batch size to work, we report the results they reported in the paper and the reproduced results under the same setting.

The results are reported in Table I. As seen, the models trained by NCMI outperform those trained by the benchmark methods. Importantly, the improvement is consistent across various model sizes.

B. Experiments on ImageNet

ImageNet [9] is a large-scale image recognition dataset that contains around 1.2M training samples and 50K validation images. We have conducted experiments on two models from the ResNet family, namely ResNet-50 and ResNet-101, and

TABLE II

TOP-1 AND TOP-5 VALIDATION ACCURACY ON IMAGENET FOR MODELS TRAINED WITH NCMI AND BASELINE METHODS. CC DENOTES GREEDY PREDICTION VIA CENTROID COMPARISON; LP DENOTES LINEAR PROBING. THE BEST AND SECOND-BEST RESULTS ARE SHOWN IN **BOLD** AND UNDERLINED, RESPECTIVELY.

Method	ImageNet			
	ResNet-50		ResNet-101	
	Top-1	Top-5	Top-1	Top-5
CE	76.24	92.42	78.42	95.35
LS	78.37	94.83	79.10	96.46
Focal Loss	78.11	94.64	79.75	94.66
SupCon	63.78	86.60	67.43	90.24
SupCon (large BS)	78.70	94.30	79.33	94.52
NCMI-CC (ours)	79.01	<u>95.34</u>	79.97	96.64
NCMI-LP (ours)	<u>78.92</u>	96.23	<u>79.83</u>	<u>96.55</u>

TABLE III

TEST F1 SCORE AND AUC ON CAMELYON-17 AND BRACS DATASET FOR MODELS TRAINED WITH NCMI AND BASELINE METHODS. LP DENOTES LINEAR PROBING.

Dataset	CAMELYON-17		BRACS	
	Method	F1 score \uparrow	AUC \uparrow	F1 score \uparrow
ABMIL	0.522	0.853	0.680	0.866
+NCMI-LP	0.567	0.892	0.701	0.872
TransMIL	0.554	0.792	0.631	0.841
+NCMI-LP	0.582	0.853	0.662	0.878
AEM	0.647	0.887	0.742	0.905
+NCMI-LP	0.663	0.907	0.779	0.918
ASML	0.689	0.898	0.781	0.914
+NCMI-LP	0.710	0.914	0.824	0.936

evaluated NCMI’s performance against CE, LS, Focal Loss, and SupCon. Similar with the CIFAR-100 setting, we use an SGD optimizer with momentum of 0.9 learning rate of 0.5, weight decay of 5e-5 and batch size of 1024, we train the models with 1000 epochs, with cosine annealing learning rate decay. For all the methods, we train the model using the image resolution of 224×224 , while at evaluation, we apply a resolution of 280×280 . For SupCon, we report the results under the same setting as all other methods and those presented in their paper.

C. Experiments on Whole Slide Image Dataset

To assess NCMI beyond natural images, we evaluate on two whole-slide image (WSI) classification benchmarks: CAMELYON-17 [28] and BRACS [11]. CAMELYON-17 comprises 1000 WSIs from five medical centers, providing a diverse and clinically representative cohort. Of these, 500 slides are publicly available with slide-level labels, while the remaining 500 are held out for challenge evaluations. The multi-institutional composition introduces substantial variation in staining and scanning, making CAMELYON-17 a strong test bed for generalization. BRACS is a large-scale WSI dataset curated for breast cancer subtype classification, comprising 547 WSIs collected from several institutions and annotated by expert pathologists into clinically relevant categories: benign tumors, atypical tumors, and malignant tumors. We follow the official split of each dataset into training, validation, and test sets.

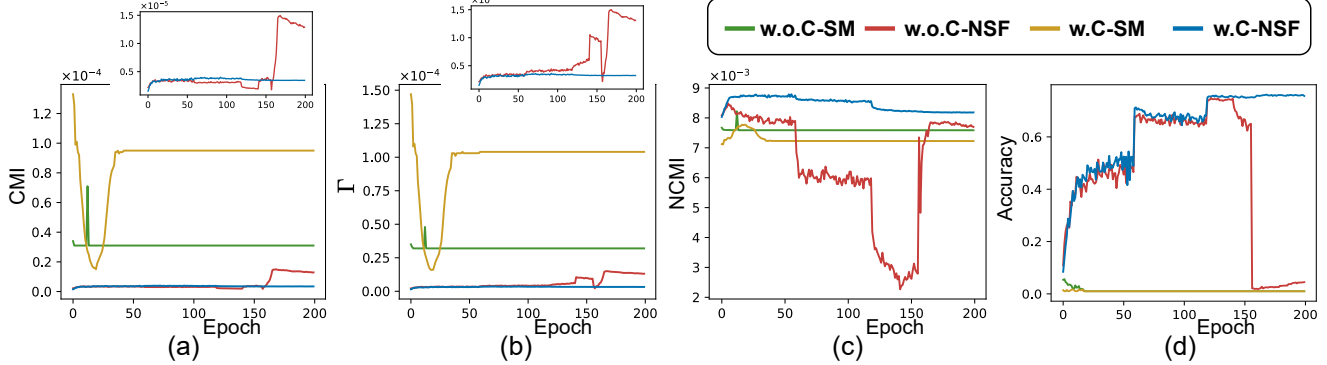


Fig. 4. The evolution curves of ResNet-18 on CIFAR-100 under all combinations of NSF and feature centering (enabled/disabled). Shown are the epoch-wise trajectories of (a) CMI, (b) Γ , (c) NCMI, and (d) accuracy.

TABLE IV
PER-EPOCH WALL-CLOCK TIME AND PEAK GRAPH MEMORY FOR RESNET-50 AND RESNET-101 ON IMAGENET.

ImageNet				
	ResNet-50		ResNet-101	
	Time ↓	Memory ↓	Time ↓	Memory ↓
CE	6 mins 39 s	102.29 Gb	10 mins 33 s	142.67 Gb
Focal Loss	6 mins 42 s	104.63 Gb	10 mins 35 s	143.42 Gb
SupCon	9 mins 52 s	180.32 Gb	16 mins 03 s	241.17 Gb
NCMI (ours)	6 mins 44 s	107.89 Gb	10 mins 49 s	148.55 Gb

We compare four state-of-the-art multiple instance learning methods, namely, ASMIL [29], TransMIL [30], ABMIL [31] and AEM [32]. For each method, we remove the classification head and train with the NCMI surrogate loss. Then, we apply linear probing to all methods. Because both datasets are class-imbalanced, we use macro-averaged AUC and macro-averaged F1 as the primary metrics. Results in Table III show that replacing cross-entropy with NCMI consistently improves both F1 and AUC on CAMELYON-17 and BRACS.

D. Training Cost & Training Stability

Compared with SupCon, NCMI uses less GPU memory and trains faster because it requires only a single forward pass and a simple objective. We quantify these efficiency gains on ImageNet in Table IV, reporting per-epoch wall-clock time and peak GPU memory usage. For fairness, all experiments were conducted on a server with two *AMD EPYC 7763 CPUs* and eight *NVIDIA A5000 GPUs*, using the same optimizer and data pre-processing, with batch size of 1024. As seen, compare with SupCon, NCMI only take 59.83% of the graphic memory, on par with the CE and Focal Loss, while largely outperform all the baselines in terms of classification accuracy.

NCMI also converges reliably with small batches. Figure 3 shows how batch size affects the validation accuracy of CE, SupCon, and NCMI. We train ResNet-50 on CIFAR-100 with batch sizes {16, 32, 64, 128, 256, 1024}. Across all batch sizes, NCMI exhibits robust convergence and consistently surpasses CE. Furthermore, we observe that SupCon relies heavily on large batches; reducing the batch size results in a significant decline in accuracy.

VI. ABLATION STUDY

To understand the design choice, in this section, we evaluate the effects of the NSF and feature centering on the CIFAR-100

TABLE V
COMPONENT-WISE ABLATION OF NCMI ON CIFAR-100. WE EVALUATE THE CONTRIBUTION OF THE NSF AND THE CENTERING OPERATION.

CIFAR-100				
NSF	✓	✓	✗	✗
Centering	✓	✗	✓	✗
Accuracy	76.45	74.9	1.72	5.64

dataset by enabling and disabling them in all possible combinations, as shown in Table V. Removing either component degrades performance, with the NSF having the larger impact. Replacing the NSF with a softmax head causes the model to fail to converge to a non-trivial solution.

To understand how these components affect learning, we visualize the ResNet-18 training trajectories of CMI, Γ , NCMI, and accuracy on the CIFAR-100 test set in Figure 4. As shown, the NSF plays a pivotal role in NCMI training: when the softmax function is used to map features to probability distributions, the model fails to converge. Feature centering further stabilizes training. Specifically, with the NSF enabled but without centering, the model collapses around epoch 150; after centering is enabled, it converges properly. Due to the space limit, we further evaluate the effectiveness of NSF and the centering operation by visualizing class clusters and their centers in the appendix.

VII. CONCLUSION

In this paper, we present a new surrogate loss for DNN-based classifiers, called normalized conditional mutual information (NCMI). We further propose a novel alternating learning algorithm to minimize the NCMI loss to train a DNN-based classifier. Extensive experiment results over natural images and WSI datasets consistently show that DNN-based classifiers trained with NCMI outperform those trained using other CE-based or heuristic loss functions.

Open questions include: (1) how to extend the CMI and Γ with multiple centroids per class to further improve the learning process, (2) how to develop a robust version of NCMI to improve adversarial robustness, and (3) how to extend NCMI to the natural language process under auto-regression pretraining. We leave these problems for future work.

REFERENCES

[1] D. R. Cox, “The regression analysis of binary sequences,” *Journal of the Royal Statistical Society Series B: Statistical Methodology*, vol. 20, no. 2, pp. 215–232, 1958.

[2] E.-H. Yang, S. M. Hamidi, L. Ye, R. Tan, and B. Yang, “Conditional mutual information constrained deep learning for classification,” *IEEE Transactions on Neural Networks and Learning Systems*, 2025.

[3] K. Ranasinghe, M. Naseer, M. Hayat, S. Khan, and F. S. Khan, “Orthogonal projection loss,” in *Proceedings of the IEEE/CVF international conference on computer vision*, 2021, pp. 12 333–12 343.

[4] L. Hui, M. Belkin, and S. Wright, “Cut your losses with squentropy,” in *International Conference on Machine Learning*. PMLR, 2023, pp. 14 114–14 131.

[5] P. Khosla, P. Teterwak, C. Wang, A. Sarna, Y. Tian, P. Isola, A. Maschinot, C. Liu, and D. Krishnan, “Supervised contrastive learning,” *Advances in neural information processing systems*, vol. 33, pp. 18 661–18 673, 2020.

[6] A. v. d. Oord, Y. Li, and O. Vinyals, “Representation learning with contrastive predictive coding,” *arXiv preprint arXiv:1807.03748*, 2018.

[7] L. Hui and M. Belkin, “Evaluation of neural architectures trained with square loss vs cross entropy in classification tasks,” in *International Conference on Learning Representations*, 2021. [Online]. Available: <https://openreview.net/forum?id=hsFN92eQElA>

[8] A. Krizhevsky, G. Hinton *et al.*, “Learning multiple layers of features from tiny images,” *University of Toronto*, 2009.

[9] J. Deng, W. Dong, R. Socher, L.-J. Li, K. Li, and L. Fei-Fei, “Imagenet: A large-scale hierarchical image database,” in *2009 IEEE Conference on Computer Vision and Pattern Recognition*, 2009, pp. 248–255.

[10] P. Bandi, O. Geessink, Q. Manson, M. Van Dijk, M. Balkenhol, M. Hermsen, B. E. Bejnordi, B. Lee, K. Paeng, A. Zhong *et al.*, “From detection of individual metastases to classification of lymph node status at the patient level: the camelyon17 challenge,” *IEEE transactions on medical imaging*, vol. 38, no. 2, pp. 550–560, 2018.

[11] N. Brancati, A. M. Anniciello, P. Pati, D. Riccio, G. Scognamiglio, G. Jaume, G. De Pietro, M. Di Bonito, A. Foncubierta, G. Botti *et al.*, “Bracs: A dataset for breast carcinoma subtyping in h&e histology images,” *Database*, vol. 2022, p. baac093, 2022.

[12] E. Oyallon, “Building a regular decision boundary with deep networks,” in *Proceedings of the IEEE Conference on Computer Vision and Pattern Recognition*, 2017, pp. 5106–5114.

[13] V. Papyan, “Traces of class/cross-class structure pervade deep learning spectra,” *Journal of Machine Learning Research*, vol. 21, no. 252, pp. 1–64, 2020. [Online]. Available: <http://jmlr.org/papers/v21/20-933.html>

[14] V. Papyan, X. Han, and D. L. Donoho, “Prevalence of neural collapse during the terminal phase of deep learning training,” *Proceedings of the National Academy of Sciences*, vol. 117, no. 40, pp. 24 652–24 663, 2020.

[15] J. Zarka, F. Guth, and S. Mallat, “Separation and concentration in deep networks,” in *International Conference on Learning Representations*, 2021. [Online]. Available: <https://openreview.net/forum?id=8HhkbjrWLdE>

[16] K. Ranasinghe, M. Naseer, M. Hayat, S. Khan, and F. S. Khan, “Orthogonal projection loss,” in *Proceedings of the IEEE/CVF International Conference on Computer Vision (ICCV)*, October 2021, pp. 12 333–12 343.

[17] T.-Y. Lin, P. Goyal, R. Girshick, K. He, and P. Dollár, “Focal loss for dense object detection,” in *Proceedings of the IEEE international conference on computer vision*, 2017, pp. 2980–2988.

[18] Z. Leng, M. Tan, C. Liu, E. D. Cubuk, J. Shi, S. Cheng, and D. Anguelov, “Polyloss: A polynomial expansion perspective of classification loss functions,” in *International Conference on Learning Representations*, 2022. [Online]. Available: <https://openreview.net/forum?id=gSdSJoenupI>

[19] C. Szegedy, V. Vanhoucke, S. Ioffe, J. Shlens, and Z. Wojna, “Rethinking the inception architecture for computer vision,” in *Proceedings of the IEEE conference on computer vision and pattern recognition*, 2016, pp. 2818–2826.

[20] R. Müller, S. Kornblith, and G. E. Hinton, “When does label smoothing help?” *Advances in neural information processing systems*, vol. 32, 2019.

[21] D. Katsikas, N. Passalis, and A. Tefas, “Inducing neural collapse via anticlasses and one-cold cross-entropy loss,” *IEEE Transactions on Neural Networks and Learning Systems*, pp. 1–12, 2025.

[22] E.-H. Yang, S. M. Hamidi, L. Ye, R. Tan, and B. Yang, “Conditional mutual information constrained deep learning: Framework and preliminary results,” in *2024 IEEE International Symposium on Information Theory (ISIT)*, 2024, pp. 569–574.

[23] K. He, X. Zhang, S. Ren, and J. Sun, “Deep residual learning for image recognition,” in *Proceedings of the IEEE Conference on Computer Vision and Pattern Recognition (CVPR)*, June 2016.

[24] M. Ilse, J. Tomczak, and M. Welling, “Attention-based deep multiple instance learning,” in *International conference on machine learning*. PMLR, 2018, pp. 2127–2136.

[25] M. Caron, H. Touvron, I. Misra, H. Jégou, J. Mairal, P. Bojanowski, and A. Joulin, “Emerging properties in self-supervised vision transformers,” in *Proceedings of the IEEE/CVF international conference on computer vision*, 2021, pp. 9650–9660.

[26] M. Oquab, T. Darcret, T. Moutakanni, H. V. Vo, M. Szafraniec, V. Khalidov, P. Fernandez, D. HAZIZA, F. Massa, A. El-Nouby, M. Assran, N. Ballas, W. Galuba, R. Howes, P.-Y. Huang, S.-W. Li, I. Misra, M. Rabbat, V. Sharma, G. Synnaeve, H. Xu, H. Jegou, J. Mairal, P. Labatut, A. Joulin, and P. Bojanowski, “DINOv2: Learning robust visual features without supervision,” *Transactions on Machine Learning Research*, 2024, featured Certification. [Online]. Available: <https://openreview.net/forum?id=a68SUt6zFt>

[27] A. Paszke, S. Gross, F. Massa, A. Lerer, J. Bradbury, G. Chanan, T. Killeen, Z. Lin, N. Gimelshein, L. Antiga *et al.*, “Pytorch: An imperative style, high-performance deep learning library,” *Advances in neural information processing systems*, vol. 32, 2019.

[28] P. Bändi, O. Geessink, Q. Manson, M. Van Dijk, M. Balkenhol, M. Hermsen, B. Ehteshami Bejnordi, B. Lee, K. Paeng, A. Zhong, Q. Li, F. G. Zanjani, S. Zinger, K. Fukuta, D. Komura, V. Ovtcharov, S. Cheng, S. Zeng, J. Thagaard, A. B. Dahl, H. Lin, H. Chen, L. Jacobsson, M. Hedlund, M. Çetin, E. Halıcı, H. Jackson, R. Chen, F. Both, J. Franke, H. Küsters-Vandervelde, W. Vreuls, P. Bult, B. van Ginneken, J. van der Laak, and G. Litjens, “From detection of individual metastases to classification of lymph node status at the patient level: The camelyon17 challenge,” *IEEE Transactions on Medical Imaging*, vol. 38, no. 2, pp. 550–560, 2019.

[29] L. Ye, S. M. Hamidi, Z. Chi, G. Li, M. Pilanci, T. Ogawa, M. Haseyama, and K. N. Plataniotis, “Asmil: Attention-stabilized multiple instance learning for whole-slide imaging,” in *Under Review*, 2025.

[30] Z. Shao, H. Bian, Y. Chen, Y. Wang, J. Zhang, X. Ji, and Y. Zhang, “TransMIL: Transformer based correlated multiple instance learning for whole slide image classification,” in *Advances in Neural Information Processing Systems*, A. Beygelzimer, Y. Dauphin, P. Liang, and J. W. Vaughan, Eds., 2021. [Online]. Available: <https://openreview.net/forum?id=LKUfuWxajHc>

[31] M. Ilse, J. M. Tomczak, and M. Welling, “Attention-based deep multiple instance learning,” *arXiv preprint arXiv:1802.04712*, 2018.

[32] Y. Zhang, Z. Shui, Y. Sun, H. Li, J. Li, C. Zhu, and L. Yang, “Aem: Attention entropy maximization for multiple instance learning based whole slide image classification,” *International Conference on Medical Image Computing and Computer Assisted Intervention*, 2025.

APPENDIX

Figure 5 summarizes the effect of centering and NSF. Panel (a) shows the evolution of CMI, Γ , NCMI, and accuracy during training. Panel (b) visualizes feature clusters at epochs $\{60, 120, 200\}$ under each setting; the black crosses indicate constant-valued vectors that correspond, after σ , to the uniform distribution. Enabling centering pulls class clusters toward these reference points, thereby mitigating drift toward biased outputs. Panel (c) plots the trajectories of feature centers (and EMA-updated centers, when applicable). With centering, the centers remain stably concentrated around the constant-valued directions; without centering, they drift and collapse.

Softmax (SM) tends to produce degenerate manifolds in the t-SNE space—indicating that a few logits dominate the feature—whereas NSF suppresses overlarge entries and yields better-balanced probabilities, stabilizing optimization.

Together, NSF and centering prevent single-mode collapse and avoid output distributions dominated by a few entries, leading to a more stable and reliable training process.

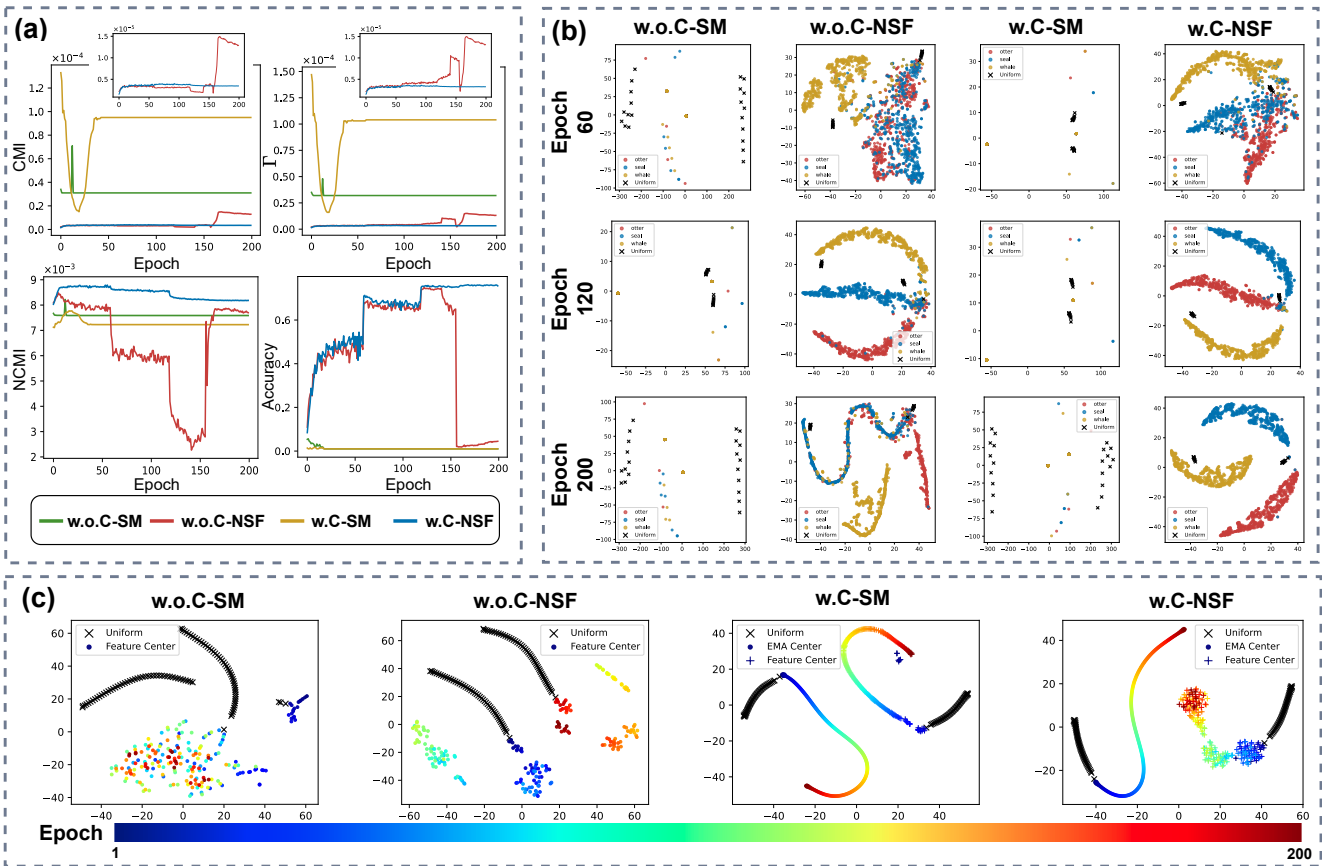


Fig. 5. Ablation of feature centering and the normalized sigmoid (NSF). We ablate each component by enabling or disabling it: **w.o.C/w.C** denote without/with centering, and **SM/NSF** denote applying softmax/normalized sigmoid function. (a) Training curves of CMI, Γ , NCMI, and top-1 accuracy for ResNet-18 on CIFAR-100. (b) t-SNE of features from three randomly selected classes at epochs 60, 120, and 200; black crosses mark constant-valued vectors (all entries equal), which map via σ to the uniform distribution. (c) t-SNE trajectories of feature centers and their EMA updates across training under all settings.